High Performance Space Lubrication of MoS2 with Tantalum

P. Serles, E. Nicholson, J. Tam, N. Barri, J.-B. Chemin, G. Wang, Y. Michel, C.V. Singh, P. Choquet, A. Saulot, et al.

High Performance Space Lubrication of MoS_2 with Tantalum

Peter Serles[1,2], Eric Nicholson[3], Jason Tam[3], Nima Barri[1], Jean-Baptiste Chemin[4], Guorui Wang[1], Yann Michel[5], Chandra Veer Singh[3], Patrick Choquet[4], Aurélien Saulot[2], Tobin Filleter[1*], Guillaume Colas[6*]*

P. Serles, N. Barri, G. Wang, T. Filleter
[1] Department of Mechanical & Industrial Engineering, The University of Toronto, 5 King's College Road, Toronto, ON, Canada, M5S 3G8

P. Serles, A. Saulot
[2] Univ. Lyon, INSA Lyon, CNRS, LaMCoS, UMR5259, 69621 Villeurbanne, France

E. Nicholson, J. Tam, C. V. Singh
[3] Department of Materials Science and Engineering, The University of Toronto, 184 College St, Toronto, ON, Canada, M5S 3E4

J.B. Chemin, P. Choquet
[4] Department of Materials Research and Technology, Luxembourg Institute of Science and Technology (LIST), 28 avenue des Hauts-Fourneaux L-4362 Esch-sur-Alzette, Luxembourg

Y. Michel
[5] Centre National D'Études Spatiales (CNES), 18 Avenue Edouard Belin, 31401 Toulouse, France

G. Colas
[6] Univ. Bourgogne Franche-Comté FEMTO-ST Institute CNRS/UFC/ENSMM/UTBM, Department of Applied Mechanics, 24 rue de l'Epitaphe, F-25000 Besançon, France

Emails: G. Colas (guillaume.colas@femto-st.fr), T. Filleter (filleter@mie.utoronto.ca), A. Saulot (aurelien.saulot@insa-lyon.fr)

Keywords: Molybdenum Disulfide, Lubricant, Space, Tantalum, Ultra-high vacuum

Molybdenum disulfide coatings have been employed as lubricants for spacecraft since the 1950s but continue to face major engineering challenges including performance in both terrestrial air and deep space vacuum environments and service lifetimes on the order of decades without maintenance. Co-deposition of MoS_2 with additive compounds has led to improvements in some circumstances but a lubricant which can perform in all space-facing environments with long lifetimes remains an ongoing problem. Herein, we demonstrate the multi-environment adaptable performance of a novel MoS_2 + tantalum lubricant coating which excels as a lubricant in both terrestrial and space environments while the benchmark space-qualified commercial MoS_2 lubricants coatings do not. It is noted that the 10% tantalum additive exhibits preferential oxidation in air to preserve the lubricating ability of MoS_2 while forming phases of TaS_2 which aid in the exceptional lubrication of MoS_2 in ultra-high vacuum. Additionally, completely different tribofilms of small particles and compact sheets are noted for air and vacuum environments, respectively, which allows for adaptable lubricating mechanisms from a single coating depending on the environment. This novel coating sets the benchmark as the first demonstrated instance of a fully versatile space lubricant which offers high-performance in both terrestrial and deep space environments.

1. Introduction

Space-bound robotics from telescopes to rovers consist of an enormous variety of mechanisms such as bearings, reaction wheels, and harmonic drive gears. These mechanisms must operate with ultrahigh precision for the entire lifetime of the mission and, as their service life can occur hundreds to millions of kilometers from earth, without the possibility of maintenance. This makes lubrication an essential component of all space-bound mechanisms. But, as an engineering design challenge, lubrication includes many problems that are unique to space; microgravity, extreme temperatures, and multiple forms of radiation[1,2] are just a few of the major challenges which face space-bound mechanisms that can result in mechanism failure or even catastrophic mission failures.[3–6] One of the most notable challenges for these space-bound mechanisms is the ability to perform in both humid terrestrial environments during assembly and qualification and in the ultra-high vacuum environments of outer and deep space, not to mention the rigors of launch in between.

Historically, molybdenum-disulfide (MoS_2) has been employed as a space lubricant due to its affinity for vacuum environments.[7,8] However, it is well established that the performance of MoS_2 breaks down in humid air environments due to oxidation to MoO_3 and disruption of van der Waals sliding.[9–12] Additionally, while MoS_2 lubricants were able to meet the requirements of early spacecraft, longer mission durations continue to push the demands placed on these lubricants requiring ultrahigh wear lives on the order of decades instead of months.[13,14] To address these limitations, MoS_2 has been co-deposited with an enormous range of additives including soft metals,[15–19] hard metals,[20–24] ceramics,[25–30] and combinations of all three to form "chameleon" coatings.[31–34] Most commonly, these additives are selected based on their chemical compatibility with MoS_2 including substitution into the lattice structure, dangling edge bond passivation, and preferential oxygen bonding, as well as their mechanical performance in increasing the wear resistance of the coating.[26,35,36] However, certain additives were found to actually hinder lubrication by disrupting the natural lubricity of MoS_2 while others only improve performance in specific environments.[37,38] While effective lubrication in certain environments and conditions has been achieved, to date, no solid lubricant has been able to achieve sustainable lubrication in the full spectrum of environments and conditions faced by space-bound mechanisms. As such, the search for a space lubricant with the correct compounds which can demonstrate low friction and high wear resistance across all spacecraft-facing environments remains ongoing.

In the present study, a novel lubricant coating consisting of MoS_2 co-deposited with tantalum is evaluated in comparison to three space-grade MoS_2 lubricants of pure MoS_2, hard metal co-deposition (MoS_2+Ti), and ceramic co-deposition (MoS_2+WC). Tantalum was selected for co-deposition as it offers preferential oxidation which inhibits the formation of detrimental MoO_3 in air and instead produces Ta_2O_5 which is lubricious.[39,40] In addition, tantalum readily forms TaS_2 which is considered an effective lubricant under both vacuum and air conditions by NASA.[41–43] Experimental characterization of the lattice structure, chemical composition, and mechanical properties of MoS_2+Ta as compared to the other lubricants are used to identify the effects of the different compounds in promoting or suppressing favourable lubricating properties. The coatings are subjected to tribological testing using space-grade steel contacts

and substrates under ultra-high vacuum (UHV), ISO 5 clean room conditions, and a transition from clean room to vacuum environments akin to space-mechanism exposure during its lifetime. The coating performance can be directly related to the modified coating composition and it is seen that only the MoS_2+Ta lubricant coating is able to provide lasting lubricating under all of the tested conditions. This presents the first MoS_2 coating to achieve sustained lubrication performance over the breadth of environmental conditions for space-systems and the ability to achieve high-performance lubrication for the growing demands of spacecraft.

2. MoS_2 Co-Deposition with Tantalum

The novel MoS_2+Ta coating and three other benchmark coatings were all sputter-deposited with coating thicknesses of 0.9-1.1 µm on space-grade steel substrates (AISI 440C, 58 HRC, R_a=0.1µm) as seen in **Figure 1** A-D. The interface of MoS_2 with the steel substrate can often be a point of failure by delamination due to the abrupt change in material properties causing stress concentrations at the interface.[44] To address this, adhesion layers are often employed as seen for the thick WC layer of MoS_2+WC and very thin layers for MoS_2+Ta and MoS_2+Ti. Figure 1 E-H shows the cross-sectional high-resolution transmission electron microscopy (HRTEM) images of the four coatings inset with the selected area electron diffraction (SAED) pattern. It can be seen that while the pure MoS_2 coating has a structure of nanocrystallites in an amorphous matrix as per Figure 1E[45], the addition of tantalum or titanium produces a fully amorphous nanostructure as seen in Figure 1 F&H, respectively. Conversely, the MoS_2+WC coating is largely nanocrystalline with an apparent horizontally layered nanostructure as seen in Figure 1 G. Looking at the long-range coating microstructure (Figures 1 A-D), the MoS_2, MoS_2+Ta and MoS_2+WC coatings show vertical columnar order while the MoS_2+Ti coating shows a uniform cross-section. The coating microstructure is influenced by the sputter-deposition parameters[46] and coatings which exhibit long-range vertical order have demonstrated greater wear resistance and enhanced adhesion with the substrate, as well as rapid formation of a coherent tribofilm by feeding and trapping particles within the surface morphology.[47] As such, the MoS_2+Ta was designed with a columnar microstructure as seen in Figure 1B & **Supplementary Figure S1**.

Figure 1 I-L shows the energy dispersive X-ray spectroscopy (EDS) analysis of the coatings with tagged chemical species. It can be noted that the signal at 8.04 keV resulting from the copper TEM grid is present in all four samples. The three co-deposited coatings show the same Mo and S peaks as the pure MoS_2 coating with the addition of Ta-Lα and Ta-M peaks in Figure 1J, W-Lα and W-M peaks in Figure 1K, and Ti- Kα peak in Figure 1L. The relative atomic proportion of the additive elements are 8% Ti, 7% WC, and 10% Ta in the respective coatings and homogeneously distributed throughout its thickness (**Supplementary Figure S2-4)**. The 10% additive concentration of Ta in the coating was designed as prior studies have indicated optimal ranges for additive concentrations to be between 5-10%[48] and have shown lubricant failure at doping concentrations beyond 13.5% for Ti.[49]

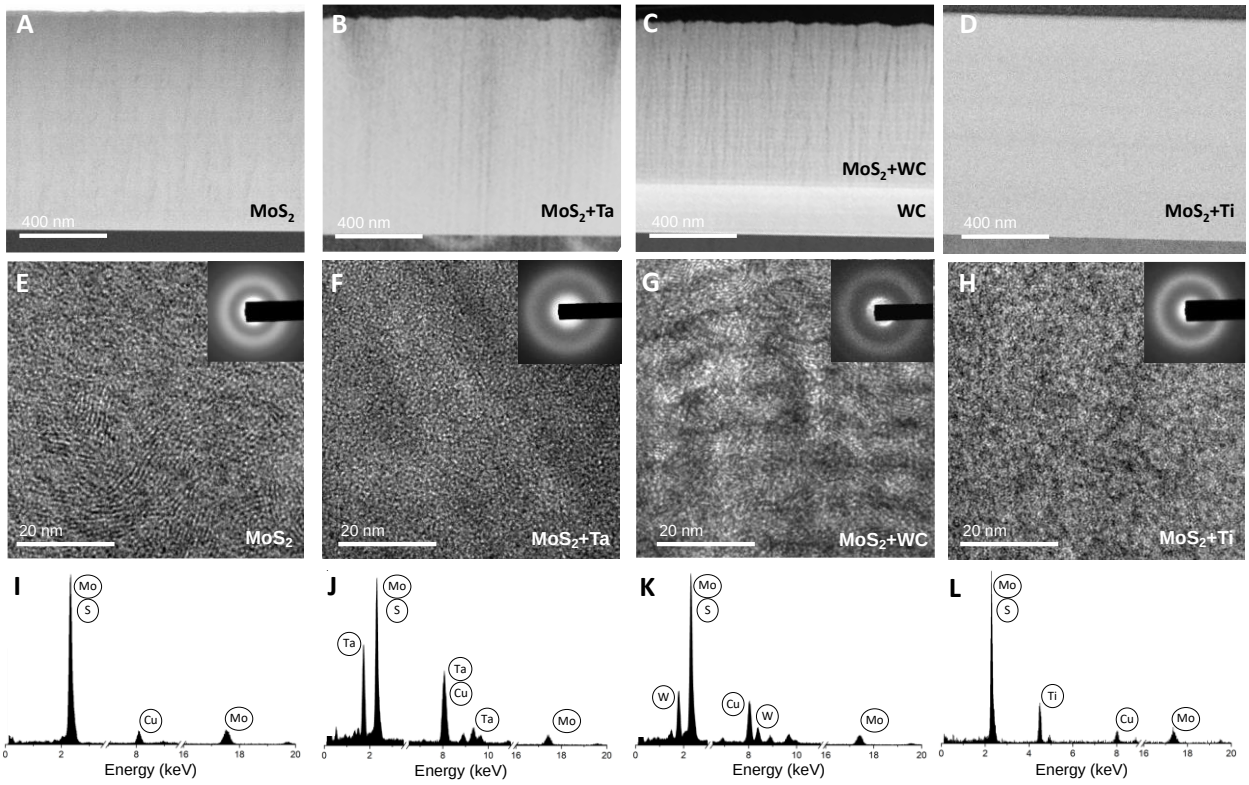

Figure 1. Cross-sectional TEM analysis of the four MoS_2-based coatings. High angle annular dark field images of the whole coating cross-section for **A.** MoS_2, **B.** MoS_2+Ta, **C.** MoS_2+WC, **D.** MoS_2+Ti. HRTEM and SAED inset showing nanocrystalline or amorphous structures for **E.** MoS_2, **F.** MoS_2+Ta, **G.** MoS_2+WC, **H.** MoS_2+Ti. Spectra from EDS elemental analysis with relevant species labelled for **I.** MoS_2, **J.** MoS_2+Ta, **K.** MoS_2+WC, **L.** MoS_2+Ti. Note: Cu-Kα signal at 8.04 keV is apparent in all samples from the TEM grid.

3. Lubrication Under Ground to Deep Space Conditions

The four coatings were evaluated using a load-controlled tribometer in linear reciprocating motion at 1 GPa maximum Hertz contact pressure with an AISI 440C steel contact. The substrate and counter-face are both AISI 440C steel akin to the standard materials of ball bearings, races, and harmonic drives for space systems[50,51]. The tests were run to 1000 cycles or until the coating failed (coefficient of friction μ>0.5) under ultra-high vacuum (UHV, 2.7±1.2 10^{-6} Pa), humid air (ISO 5 clean room, RH 43±5%), and with an environmental transition (150 cycles Air/850 cycles UHV) to closely mimic environments faced by space-systems. Further UHV tribometer details can be found in Methods[47,52]. The coefficient of friction as an average of each cycle and test is seen in **Figure 2** A-C for the three environments.

Under the UHV environment in Figure 2A, the impressive lubricating ability of pure MoS_2 is apparent with the lowest and most stable friction behaviour of μ=0.029±0.002 throughout the entire 1000 cycles. The novel MoS_2+Ta coating as well as the space-qualified WC co-deposit coating also perform extremely well under UHV with low friction coefficients of μ=0.083±0.08 and μ=0.056±0.002 respectively. The MoS_2+Ti coating, however, is found to fail under UHV

with the friction sharply increasing after 225 cycles corresponding with coating depletion similarly to prior studies.[20,37,53–55] Prior to this failure, the MoS_2+Ti coating has the lowest friction coefficient of μ=0.023±0.004 which suggests strong lubricating performance but with a low wear resistance making it well suited to one-shot mechanisms such as the opening of solar panels or possibly short to medium life high precision mechanisms such as telescope focusing mechanisms.

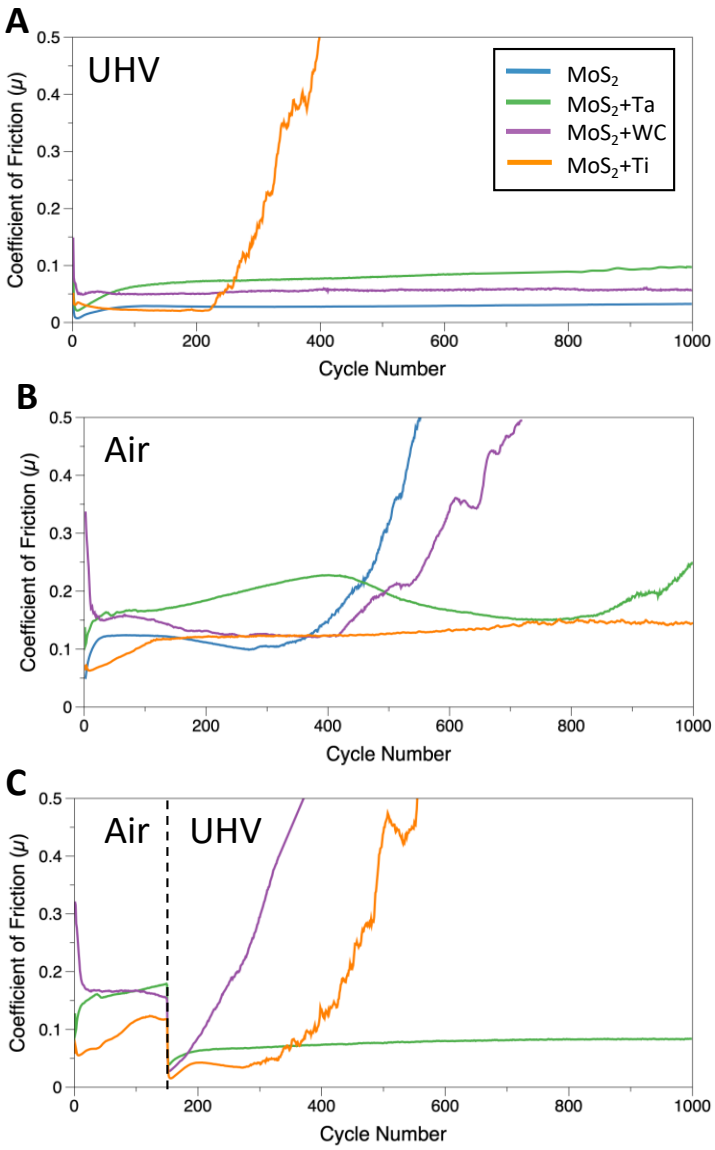

Figure 2. Tribological testing of the pure and co-deposited MoS_2 coatings. Per-cycle averaged friction coefficient under **A**. Ultra-high vacuum (2.7 ± 2.2 10^{-6} Pa), **B**. Humid clean-room air (ISO 5 Clean Room, RH 43±5%), **C**. Transition from 150 cycles under air condition followed by pumping down the chamber and 850 cycles in UHV

The tribological testing under humid air, representative of terrestrial preparation, qualification, testing, and launch, shows a different story as seen in Figure 2B. Space mechanisms are typically stored in minimum ISO 5 grade clean rooms[56–58] to protect from contaminants but these environments nonetheless include ambient humidity. High humidity is well known to

detriment lubrication performance of MoS_2 due to oxide generation (MoO_3) which is covalently bonded and brittle thus interrupting the lubricious capabilities of MoS_2 in dry and vacuum environments.[12,20,59] As a result, all four of the coatings are seen to exhibit higher friction forces in the range of μ=0.1 to 0.2, and MoS_2 is found to fail quickly beginning at cycle 320. However, the co-deposited MoS_2+Ta coating is found to endure the entire 1000 cycles with a controlled friction coefficient of $\mu \leq 0.22$. The only other coating which survives the 1000 cycles in air is the MoS_2+Ti coating which suggests the additive transition metals play a significant role in the coating composition and resulting performance. The MoS_2+WC coating has been previously noted to consist of independent MoS_2 and WC nanocrystallites[25,26] which does little to protect the MoS_2 from oxidation and coating failure is thus noted beginning at cycle 415 for MoS_2+WC similarly to previous studies on this coating.[60]

To consider the full suite of space-facing environments, the MoS_2+Ta coating and two commercial co-deposited coatings were subjected to a transition of environments from 150 cycles in air to 850 cycles in UHV as a surrogate for the transition of environments from terrestrial to deep space. It can be seen in Figure 2C that only the MoS_2+Ta coating is able to survive all 1000 cycles, with an average coefficient of friction similar to that of the UHV test. This implies that the contact properties from operation under air rapidly transition to fit UHV lubrication requirements as the coating adapts to performance under UHV. Conversely, both MoS_2+Ti and MoS_2+WC fail following the transition to UHV; the MoS_2+WC coating begins to fail beginning immediately after the transition while the MoS_2+Ti coating begins to fail after 200 cycles in UHV. Wear trends which match these lifetimes can be noted by the *in situ* optical images of the wear tracks (**Supplementary Figure S5**). While MoS_2+Ta shows some wear particles in air, the majority of the wear under UHV occurs during the first 40 cycles following the transition (cycles 150-190) as compared to the 800 following cycles (190-990) which suggests the formation of a stable lubricating state upon reaching UHV. For MoS_2+Ti, fewer ejected wear particles can be noted during the first 150 cycles under air but significant wear occurs rapidly under UHV. Conversely, MoS_2+WC shows significant wear during the air cycles which leads to coating depletion and visibility of the WC adhesion layer and thus rapid failure after transition. Of the three co-deposited coatings, only MoS_2+Ta is able to survive the transition of environments which is akin to its strong performance in the air and UHV conditions individually and is indicative of its suitability as a high-performance space lubricant.

4. Lubricating Mechanisms

The rheology and granularity of the tribofilm provides mechanical insights into the lubricating mechanisms of the contact. **Figure 3** A-K and **Supplementary Figure S6&7** shows secondary electron scanning electron microscopy (SEM) images of the four coatings and the ejected wear debris after testing in the three environments. The schematic in Figure 3L shows the region of interest where the SEM images have been taken at the edge of the wear track where the majority of ejected debris accumulates. The corresponding images of the steel counter-face show similar tribofilm rheology (**Supplementary Figure S8**) and **Supplementary Figure S9&10** shows EDS maps of the tribofilms confirming the films are made of recirculated coating material. It

can be seen in Figure 3 A-K that the wear scars, tribofilms, and wear debris vary widely based on the coating and further show significant variation for the same coating performing under different environments.

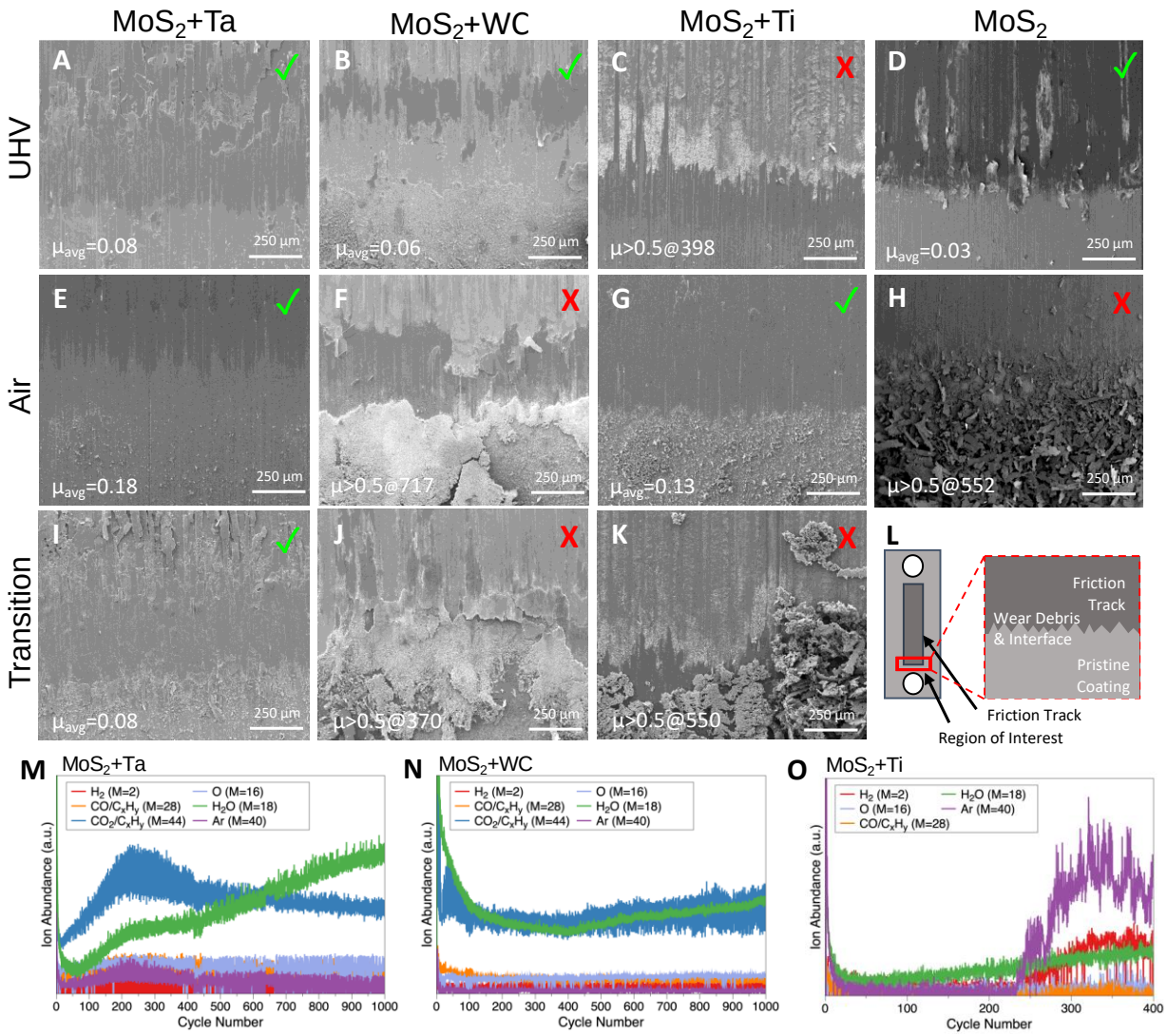

Figure 3. SEM images of the four coatings following 1000 cycles or failure (μ>0.5) in the three environments; MoS_2+Ta, MoS_2+WC, MoS_2+Ti, and MoS_2 respectively in **A-D**. Ultra-High Vacuum, **E-H**. Air and **I-K**. Transition from Air to UHV, and **L**. Schematic of SEM image location on the wear track. **M-O.** Mass spectrometry of desorbed species during UHV testing of MoS_2+Ta, MoS_2+WC, and MoS_2+Ti, respectively.

Under the UHV environment, the three coatings which successfully lubricate the contact all appear to form a coherent smooth tribofilm of sheet-like films within the wear scar while the MoS_2+Ti coating, which experiences failure, consists predominantly of small particles and a very rough surface in the wear scar. This can be further illustrated by considering the *in situ* mass spectrometry of the three co-deposited coatings in Figure 3 M-O. Spacecraft experience desorption of water, nitrogen and carbon compounds, halogens, and hydrocarbons even years after launch as components are operated, worn, or exposed to new conditions throughout the mission lifetime.[61,62] In the present case, all desorbed species result directly from the coating operation as the tribometer is mechanically voided prior to operation (*cf.* Methods). It is seen

that all three coatings desorb predominantly carbon oxides, hydrocarbons, and H_2O species into the UHV atmosphere during lubricant operation which corresponds with desorption of internal trapped compounds proportionally to the friction coefficient and wear rates.[47] As such, all three mass spectra show high initial rates of CO_2/C_xH_y and H_2O desorption corresponding to increased friction and wear during run-in.[47] However, following run-in the MoS_2+Ta and MoS_2+WC desorption rates are stable which suggests these contacts achieve a sustainable low-wear regime. Conversely, MoS_2+Ti shows high H_2O desorption rates throughout its lifetime before showing Ar and H_2 desorption beginning at cycle 225 which corresponds with complete coating failure.[37] The formation of a stable tribofilm and contact for MoS_2+Ta and MoS_2+WC following run-in thus acts to successfully accommodate the friction forces of the contact which leads to a sustainable low-wear regime. Meanwhile the small particles produced in the MoS_2+Ti contact do not form a stable coverage of the underlying film which leads to high wear rates and complete coating depletion after only 225 cycles.

The opposite behaviour is noted in the air environment as the coatings which survive the 1000 cycles show a predominance of small particles (MoS_2+Ta and MoS_2+Ti) while those that show sheet or ribbon-like tribofilms are found to fail (MoS_2+WC and MoS_2). Considering the Velocity Accommodation Theory,[63] the coherent sheet-like tribofilms are postulated to exhibit shear mode accommodation while the small particles are characteristic of rolling and rheological accommodation modes as discussed in previous works on MoS_2 and MoS_2+Ti.[20,47] As humid environments typically act to interrupt internal shear modes through oxidation and meniscus forces, this may be a contributing reason for sheet-like tribofilms failing in air conditions for MoS_2+WC and MoS_2. Meanwhile, small particle tribofilms would act to lower the total contact area, helping to mitigate the increased adhesion of MoS_2 with steel at high humidity.[64]

Of particular note, it can be seen that for the three commercial coatings, the tribofilm morphology is consistent between the UHV and air environments; MoS_2+Ti shows exclusively small particle debris which allows it to perform in air but not UHV, while MoS_2+WC and MoS_2 show sheet-like tribofilms allowing them to perform in UHV but not air. However, the MoS_2+Ta coating shows two different tribofilm behaviours specific to the two environments; the tribofilm is sheet-like in UHV but small particles in air which allows it to effectively lubricate in both environments. Looking at the transition environment behaviour, MoS_2+Ta shows signs of both sheets within the wear scar and ejected particles below suggesting an effective "adaptability" of the tribofilm for the different environments. This indicates that in order to achieve high performance lubrication across multiple environments, the lubricant must be able to exhibit multiple lubricating regimes individual to each environment. This adaptability is unique to the MoS_2+Ta coating and is the primary example of a truly versatile MoS_2 lubricant coating.

To further understand the high-performance lubrication of the MoS_2+Ta coating, the coating mechanical properties, microstructure, and composition are evaluated. The Young's modulus (EIT) and hardness (HIT) of the four coatings were measured by nanoindentation using a Berkovich diamond indenter and can be seen in **Figure 4A and Supplementary Figure S11**. While the pure MoS_2 coating exhibits a Young's modulus of 62 GPa and a hardness of 3.6 GPa,

the ≤10% portion of additives in the co-deposited coatings are able to greatly increase the Young's modulus above 95 GPa and the hardness above 6.5 GPa. The MoS_2+Ta coating shows the greatest increase in mechanical properties with E=114.2±9 GPa and H=6.65±0.4 GPa. These two mechanical properties have been related to the wear resistance of solid lubricant coatings[65,66] which may suggest enhanced tribological lifetimes for the co-deposited coatings as compared to the pure MoS_2. The similar mechanical properties between the co-deposited coatings, however, indicate that the material tribochemistry and structure likely play greater roles in the coating performance.

The modifications of the coating structures by co-deposition are further evaluated by Raman spectroscopy as shown in Figure 4B. The four phonon modes can be identified as the E^1_{2g} in-plane mode, A_{1g} out-of-plane mode, and the two LA(M) defect modes for MoS_2[67]. While pure MoS_2 is dominated by the A_{1g} and E^1_{2g} peaks, the MoS_2+Ta and MoS_2+Ti spectra show neither peak and instead show a prominent 2LA(M) defect peak. It should be noted that amorphous MoS_2 is not Raman active which indicates that no order persists within the coating.[68] The prominence of the 2LA(M) peak in these two spectra indicates that the Ta and Ti atoms have penetrated within the MoS_2 lattice to produce a modified structure as previously proposed for MoS_2+Ti.[21] Conversely, the MoS_2+WC coating shows prominent A_{1g} and E^1_{2g} peaks which indicates that the MoS_2 structure is largely unaffected by the WC. This is in agreement with the mechanical properties of the three coatings wherein the relative increase in Young's moduli for MoS_2+Ta and MoS_2+Ti are significantly greater than the values that would be expected by the rule of mixtures as noted by the dotted grey line in Figure 4A. Meanwhile, the modulus of MoS_2+WC is found to be lower than the value predicted by the rule of mixtures which suggests little interaction between the WC and MoS_2 as in agreement with previous reports of independent MoS_2 and WC phases.[25,26]

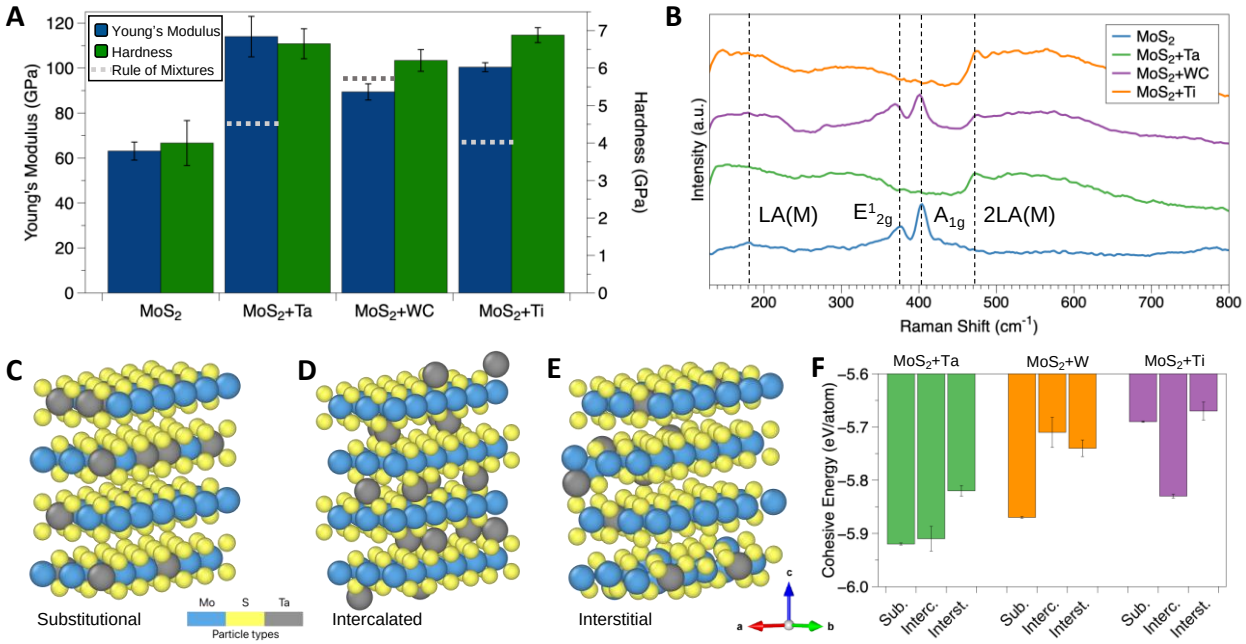

Figure 4. Structural properties of the four MoS_2 coatings. **A.** Young's modulus and hardness values for the four coatings as determined by 50 diamond tip Berkovich nanoindentation measurements, grey dotted line corresponds to the Young's modulus as determined by the rule of mixtures weighted mean. Error bars represent the standard deviation of measurements. **B.** Raman spectra for the four coatings

averaged across three scans. **C, D, E.** Representative DFT energy minimized atomic schematics of 7% tantalum in substitutional, intercalated, and interstitial states, respectively. **F.** DFT calculations of cohesive energy for substitutional, intercalated, and interstitial additive states of Ta, W, and Ti in MoS_2, respectively.

To elucidate the modified structures of these MoS_2 coatings with the incorporation of additives, density functional theory (DFT) calculations of the energetic stability for various atomic positions of Ta, Ti, and W additives in MoS_2 are presented in Figure 4 C-F. Renevier *et al.*[21] discussed the role of titanium in MoS_2 and predicted three possible atomic configurations: i) substitution for molybdenum in the matrix forming phases of TiS_2, ii) interstitial solid solution of titanium in the (100) or (010) directions, or iii) intercalation of titanium atoms between the MoS_2 layers. Examples of these three atomic configurations are shown for 7% Ta in Figure 4 C-E and the calculated cohesive energy is shown in Figure 4 F for the three coatings where lower cohesive energy is more energetically favourable. Additional calculations at other concentrations and full data are shown in **Supplementary Figure S12**.

It can be seen that each of the additives has a different preferred atomic state in MoS_2; W is more easily substituted for Mo forming phases of WS_2 while Ti is more likely to be intercalated between the sheets of MoS_2. Interestingly, Ta shows similar energetic stability in intercalated and substituted phases suggesting both states are favourable. Using Bader charge analysis (**Supplementary Figure S13**) we can further see that the intercalated atoms show the largest atomic charge of the three states which therefore exhibit the greatest potential for preferential oxidation. This can be related to the performance of the three coatings in the respective environments; Ta and Ti form intercalated phases which help to preferentially oxidize and inhibit MoO_3 formation in air, while Ta and W form sulfide phases by substitution which are lubricious in vacuum.[43,69] This further agrees with the Raman spectra wherein the intercalation of Ti and Ta into the MoS_2 structure leads to a disruption of the lattice which eliminates the A_{1g} and E^1_{2g} peaks in producing the LA(M) defect peaks.

The atomic bonding states for each of these co-deposited materials are further reflected in the X-ray photoelectron spectroscopy (XPS) spectra as seen in the Mo *3d*, S *2p*, and corresponding Ta *4f*, W *4f*, and Ti *2p* signals in **Figure 5 (**O *1s* and C *1s* signals *cf.* **Supplementary Figure S14)**. The standard MoS_2 bonding states are noted in the Mo *3d* and S *2p* spectra of Figure 5 A-H. Additionally, TaS_2, WS_2 and TiS_2 are further noted in the S *2p* spectra in varying amounts with corresponding signals in the respective additive transition metal spectra of Figure 5 I-K. The additive transition metal spectra show each element to be in a mix of binding energies which can be discerned as oxides and sulfides as well as a carbide phase for the tungsten.

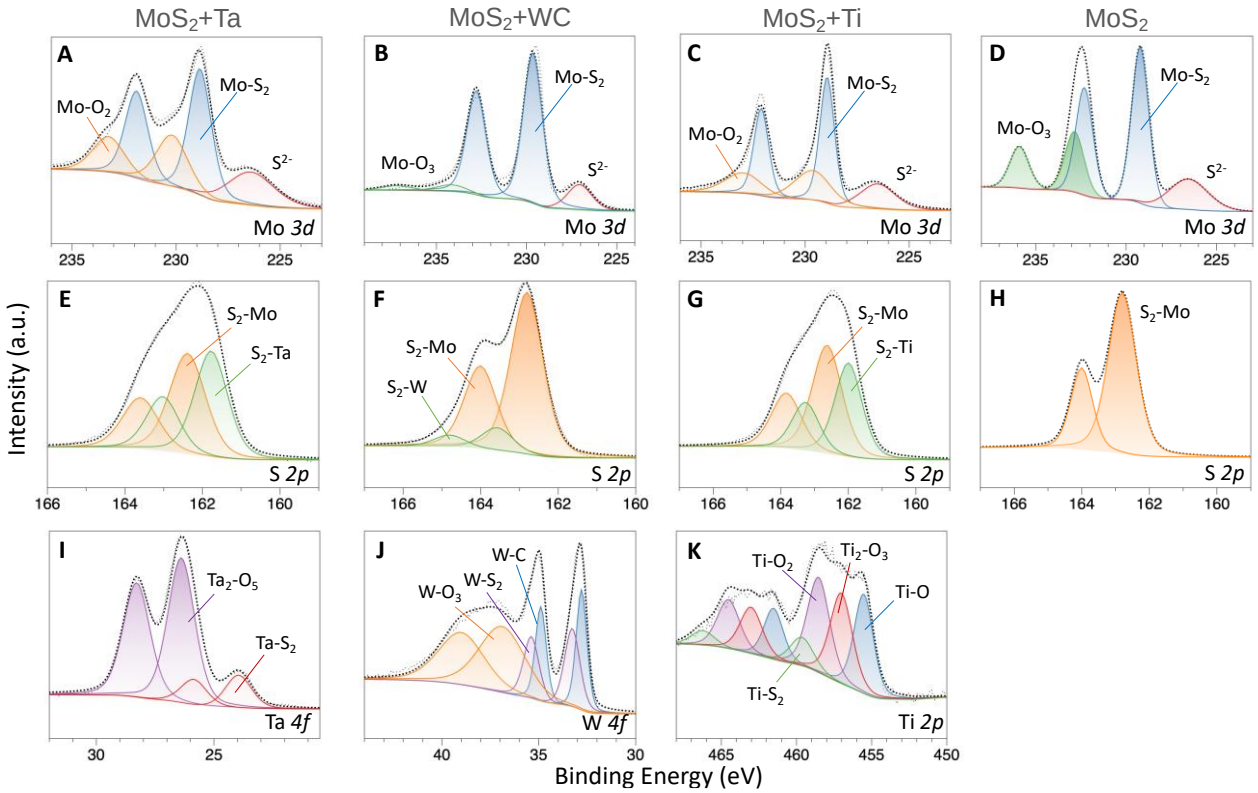

Figure 5. XPS analysis of the four MoS_2 coatings. **A-D.** Mo 3*d* signals and **E-H.** S *2p* signals for MoS_2+Ta, MoS_2+Ti, MoS_2+WC, and MoS_2 respectively. **I-K.** Ta *4f*, W *4f*, and Ti *2p* signals for the respective coatings.

It is well known that MoO_3 oxide phase is abrasive and detrimental to the performance of MoS_2 lubricants in air.[70,71] Considering Figure 5 A-D and S11 A-D, all three co-deposited coatings show a reduction in the oxide signals while pure MoS_2 shows a substantial peak. In the MoS_2+Ti coating, significant formation of titanium oxides (TiO, Ti_2O_3 and TiO_2) are noted which leads to the decrease in MoO_3 formation and effective lubrication in air as in agreement with DFT calculations.[49] However, titanium oxides are abrasive materials[72] which have demonstrated increasing friction and wear with decreasing vacuum pressure[73] resulting in ineffective lubrication in UHV conditions. Conversely, tantalum preferentially oxidizes to produce Ta_2O_5 which is commonly used as a wear resistant coating and has shown low stable friction in air.[74,75] Meanwhile, the similar energetic favorability of substitution predicted by DFT for Ta leads to significant phases of TaS_2 which is considered an effective lubricant under both vacuum and air conditions by NASA while TiS_2 has been deemed ineffective.[41–43] Interestingly, despite the poor performance of MoS_2+WC in air, the W spectra actually shows the lowest intensity of Mo oxides which is rational as W is more electronegative than Ta or Ti. However, WO_3 is a similarly abrasive compound to MoO_3 due to its monoclinic structure[76] which suggests the preferential oxidation of WO_3 instead of MoO_3 is not beneficial to the lubricating state of the coating in air. Furthermore, while DFT calculations predicted the preferential atomic state of W in MoS_2 as WS_2, XPS shows less WS_2 than WC which suggests the W is more stable as a separate WC phase which is in agreement with prior reports of MoS_2+WC.[25,26]

Due to its tribo-mechanical adaptability and its sulfide and oxide states, the MoS_2+Ta coating produces high performance lubrication in both the humid air of terrestrial environments and the

ultrahigh vacuum of deep space. The tribofilm and associated mechanical response is noted to adapt based on the environment which allows for a sustainable low-wear regime in both UHV and air, as well as the adaptability in between. Furthermore, the tantalum acts to both preferentially oxidize which reduces the degree of molybdenum oxides and additionally forms a lubricious TaS_2 phase which aids in the lubricating ability of the MoS_2+Ta coating. The various analysis techniques used herein all demonstrate that the MoS_2+Ta coating has succeeded in combining the strengths of pure MoS_2 with the chemical modification by co-deposition of tantalum producing an ideal lubricant for space mechanisms experiencing the vast rigors of space travel.

5. Conclusion

MoS_2 lubricant coatings have been employed for space applications since the 1950's but face several engineering challenges for which co-deposited compounds aim to compensate. This article demonstrates the performance of a novel MoS_2+Ta lubricant coating which is shown to excel as a lubricant in terrestrial and deep space environments while the benchmark space-grade lubricant coatings do not. It is seen that the 10% Ta additive to the sputter-deposition process for MoS_2 significantly alters the coating composition, structure, and mechanical properties to the benefit of its cross-environment lubricating performance. The tribofilms formed by MoS_2+Ta under UHV and air conditions produce different triblogical mechanisms and as a result demonstrate sustainable lubrication regardless of the environment which has not been achieved by any space lubricant to date. The enhanced coating performance in the dual environments can be further identified by the preferential formation of non-abrasive tantalum oxides rather than molybdenum oxides in air plus the formation of TaS_2 which is an effective lubricant under vacuum conditions. While the experiments demonstrated herein extend to 1000 cycles, the novel coating exhibits a stable tribofilm and shows no signs of coating depletion in either environment. This suggest significantly greater lifetimes can be achieved which will be evaluated in future studies. With the successful performance of MoS_2+Ta lubrication in both space and terrestrial environments, the next generation of spacecraft components will be able to exhibit enhanced mission performance and extended lubrication lifetimes despite the rigors placed upon them by space travel.

6. Methods

Material Synthesis

The four coatings were deposited on AISI 440C steel (58 HRC) substrates to coating thicknesses of 0.9-1.1 µm. The novel MoS_2+Ta coating was deposited by authors at the Luxembourg Institute of Science and Technology (LIST), Belvaux, Luxembourg. The coating was co-deposited by magnetron sputtering in a PVD chamber from K.J. Lesker. The pressure was maintained at $5 \cdot 10^{-3}$ mbar by an argon flow of 60 sccm. A power of 100 W and 30W was applied respectively on a MoS_2 target and a Tantalum target. Each target has a diameter of 2 inches and a purity of 99.95%. The substrate is placed at a distance of 12 cm from the target with an angle of 30° between each target and the substrate. To homogenize the coating, a

rotation of 5 rpm was maintained. The three commercially available coatings were deposited by their respective companies: pure MoS_2 coating was deposited by Blösch AG. Grenchen, Switzerland, MoS_2+Ti was deposited by Teer Coatings Ltd., Droitwich, UK, and MoS_2+WC was deposited by Tecnalia Technologies Corp, Bizkaia, Spain. The samples were tested within 2 months of deposition and were stored in ISO 5 cleanroom conditions as per NASA designated practice for space mechanisms.[56–58]

Materials Characterization

Transmission electron microscopy (TEM), Energy Dispersive X-ray Spectroscopy (EDS), and Selected Area Electron Diffraction (SAED) measurements were performed using a Hitachi HF-3300 TEM. The samples were prepared by Focused Ion Beam (FIB) liftout and thinning of the coating cross section as detailed in prior works[45]]. TEM imaging was performed using an accelerating voltage of 100 kV. The accelerating voltage were selected based on comparable literature[77,78] and appropriate precautions were taken to minimize electron beam induced artifacts.

Scanning Electron Microscopy (SEM) and EDS measurements of the tribofilms were taken using an INCA environmental SEM with an accelerating voltage of 5 kV.

High frequency Raman spectroscopy measurements were performed using a Renishaw InVia microscope with an incident wavelength of 532 nm from a diode-pumped solid-state laser. The resulting penetration depth in MoS_2 is wavelength-dependent and estimated to be around 38 nm in the case of a 532 nm laser[79]]. The laser intensity was maintained at 2% or 2 mW to avoid local heating and damage by the laser. The spectral resolution was 1.9 cm^{-1} and the spatial resolution was approximately 1 µm diameter.

X-ray Photoelectron Spectroscopy (XPS) characterization was performed at the Ontario Centre for the Characterization of Advanced Materials (OCCAM) using a Thermo Fisher Scientific K-Alpha system. Data collection and processing was performed with the Advantage package. Spectra were collected in a 900 µm box at several locations across the coating surface for binding energies of 0-1300 eV at a 1 eV resolution and detailed spectra for the peaks of interest (Figure 5 and S14) were collected with 0.1 eV resolution. Binding energy scales were shifted to centre the adventitious carbon peak at 284.8 eV. Peak fitting is done on a "Smart" background and all sub-peaks are labelled as per the National Institute of Standards and Technology (NIST) XPS Database.

Tribological Testing

Tribological testing was performed on a load-controlled reciprocating tribometer within an environmental chamber of 1 m^3. The counterface of AISI 440C steel has radii of R_x=12.5mm and R_y=500mm and is loaded to 1 GPa contact pressure. The lateral force was sampled at 300 Hz with ±0.1 N accuracy throughout the tests. Ultra-high vacuum (UHV) conditions were achieved by turbo-pumping the chamber for 24h without baking corresponding to $<10^{-6}$ Pa. Terrestrial conditions were achieved by pumping the chamber to 10^{-3} mbar and backfilling with cleanroom (ISO 5) humid air (43±5% RH). Air to UHV transition were performed by stopping the test and pumping down the chamber over 24h to $<10^{-6}$ Pa (150 cycles under humid air, 850 cycles in UHV). All tests were performed at 27 ± 3ºC and externally air cooled.

Full details regarding the design and control of the tribometer are described in [47,52]. In brief, the custom system is designed to allow for a wide variety of contact geometries (flat/flat, flat/sphere, cylinder/cylinder, etc.), sliding orientations (continuous rotation, reciprocating sliding, etc.) and conditions (ambient, UHV, lubricant-submerged, gas-filled, etc.). It is equipped with force and displacement sampling in X, Y, Z at up to 2 MHz, in situ mass spectrometry, and glass windows to view the contact during sliding. The base pressure of the system is 10^{-7} Pa which can be achieved following extended pumping of the system. Prior to

each test, the system is run for 50 cycles out-of-contact in order to desorb and vent any gasses within the mechanical components prior to operation.
The normal and lateral forces were measured throughout the test duration at 300 Hz corresponding to 3600 data points per reciprocating cycle. The friction force and normal force were averaged for each cycle and the per-cycle coefficient of friction was calculated as $\mu=F_F/F_N$. The normal force deviated by less than 0.1% from the programmed applied force throughout operation.
A PrismaPlus® QMG220 mass spectrometer is attached to the tribological chamber with a sensitivity of 1-100 amu operating with a quadruple RF tungsten filament which produces 70 eV electrons. The mass spectrometer is illuminated when operating under UHV to detect desorbed species.

Nanoindentation
Nanoindentation experiments were performed with an Anton-Paar UNHT^3 using a diamond Berkovich tip, uniform static loading to a maximum 700 µN with a loading/unloading rate of 0.06 mN/s and a 10 s dwell time at the maximum load. Impressions were made at a separation of 15 µm, substantially greater than the maximum indentation depth of 80-90 nm. Indentation load was chosen to optimize the balance of substrate and surface roughness effects, finding a penetration depth between 10% of the MoS_2 layer thickness (1.1 µm) and 20 times the surface roughness (R_a < 2 nm). Hardness (HIT) and modulus (EIT) are calculated by the Oliver and Pharr method [80] and are reported as the mean value of 25 independent tests in three areas. Uncertainties are given as the standard error under the assumption that measurements are independent and normally distributed as seen in Figure S11.

Density Functional Theory Calculations
Density functional theory calculations of the ground state energy were performed in the Vienna *ab initio* simulation package (VASP)[81] using the projector augmented wave method [82] in the Perdew-Burke-Ernzerhof formulation.[83] Kinetic energy cutoff of 350 eV is used for the wave functions. All calculations were spin-polarized and used Grimme's DFT-D3 [84] van der Waals correction term. 3x3x2 supercells of 108 atoms of MoS_2 were computed on a 2x2x1 Monckhorst-Pack[85] k-point grid centred at the gamma point. Relaxations were performed by the conjugate-gradient method to an energy difference cutoff threshold of 0.2 meV. Cohesive energy was calculated by subtracting the energy of the free ions in an identical supercell from the final energy of the relaxed defect structure. Partial charges were assigned by the Bader charge analysis as implemented by Kerrigan[86] and atomic coordinates were visualized with OVITO.[87]
Bulk 2H-MoS2 supercells were constructed starting from the Materials Project[88] mp-2815 structure and relaxing ion position and supercell size with van der Waals correction yielding cell parameters of a=0.316 nm and c=12.31 in excellent agreement with experimentally determined values. Three types of defects were considered, intercalated, interstitial and substitutional. Single impurity defects (1 at.%) were placed in several candidate locations within the lattice to find the preferred sites for intercalated and interstitial defects. The octahedral intercalated site was found to be most stable for each of the impurity elements. The interstitial defects initiated at the hollow site relaxed to several possible configurations including dumbbells or displacing the Mo atom to the hollow site. Higher concentrations of defects (4 & 7 at.%) were created at random locations using the octahedral intercalated position and the hollow site interstitial position. All structures were allowed to relax with ion positions and supercell size, and final energies were recalculated following the final supercell size adjustment. It should be noted that calculations were repeated for verification without dft-d3 correction, and without supercell size relaxation, which yielded the same observed relative trends of stability of the defect types.

Supporting Information

Supporting Information is available from the Wiley Online Library or from the author.

Acknowledgements

The authors wish to acknowledge the technical support of Sal Boccia and Peter Brodersen of the Ontario Centre for the Characterization of Advanced Materials (OCCAM) and David Leveque, Magali Busquet, and Yves Berthier of INSA-Lyon.
The authors also wish to acknowledge the Mitacs Globalink scholarship; the Canadian Foundation for Innovation; The Natural Sciences and Engineering Research Council of Canada; The Vanier Canadian Graduate Scholarship; and the French Space Agency (CNES) under contract number R&T – R-S13/TG-0002-078 for funding support.

Conflict of Interest

The authors have no conflict of interest to declare.

Received: ((will be filled in by the editorial staff))

Revised: ((will be filled in by the editorial staff))

Published online: ((will be filled in by the editorial staff))

References

[1] National Aeronautics and Space Administration, *A Researcher's Guide to the International Space Station*, **2014**.
[2] E. Nicholson, P. Serles, G. Wang, T. Filleter, J. W. Davis, C. V. Singh, *Applied Surface Science* **2021**, *567*, 150677.
[3] Space Exploration Technologies Corp. (SpaceX), **2015**.
[4] NASA, **2017**.
[5] M. Rayman, Jet Propulsion Laboratory/NASA, **2013**.
[6] R. Cowen, *Nature* **2013**, *497*, 417.
[7] T. Spalvins, *ASLE Transactions* **1969**, *12*, 36.
[8] V. R. Johnson, G. W. Vaughn, *Journal of Applied Physics* **1956**, *27*, 1173.
[9] E. Serpini, A. Rota, A. Ballestrazzi, D. Marchetto, E. Gualtieri, S. Valeri, *Surface and Coatings Technology* **2017**, *319*, 345.
[10] G. Levita, P. Restuccia, M. C. Righi, *Carbon* **2016**, *107*, 878.
[11] R. T. K. Baker, J. J. Chludzinski, R. D. Sherwood, *Journal of Materials Science* **1987**, *22*, 3831.
[12] U. Krishnan, M. Kaur, K. Singh, M. Kumar, A. Kumar, *Superlattices and Microstructures* **2019**, *128*, 274.
[13] E. W. Roberts, *Journal of Physics D: Applied Physics* **2012**, *45*, DOI 10.1088/0022-3727/45/50/503001.
[14] A. A. Voevodin, J. S. Zabinski, *Composites Science and Technology* **2005**, *65*, 741.
[15] J. R. Lince, H. I. Kim, P. M. Adams, D. J. Dickrell, M. T. Dugger, *Thin Solid Films* **2009**, *517*, 5516.

[16] P. Stoyanov, R. R. Chromik, S. Gupta, J. R. Lince, *Surface and Coatings Technology* **2010**, *205*, 1449.
[17] W. Liu, Y. Fu, X. Gao, J. Yang, J. Sun, M. Hu, L. Weng, *Vacuum* **2017**, *144*, 72.
[18] K. J. Wahl, L. E. Seitzman, R. N. Bolster, I. L. Singer, *Surface and Coatings Technology* **1995**, *73*, 152.
[19] W. D. Sun, J. Wang, K. W. Wang, J. J. Pan, R. Wang, M. Wen, K. Zhang, *Surface and Coatings Technology* **2021**, *422*, 127490.
[20] G. Colas, A. Saulot, N. Bouscharain, C. Godeau, Y. Michel, Y. Berthier, *Tribology International* **2013**, *65*, 177.
[21] N. M. Renevier, V. C. Fox, D. G. Teer, J. Hampshire, *Surface and Coatings Technology* **2000**, *127*, 24.
[22] P. Stoyanov, H. W. Strauss, R. R. Chromik, *Wear* **2012**, *274–275*, 149.
[23] R. Hauert, J. Patscheider, *Advanced Engineering Materials* **2000**, *2*, 247.
[24] X. Z. Ding, X. T. Zeng, X. Y. He, Z. Chen, *Surface and Coatings Technology* **2010**, *205*, 224.
[25] I. B. and J. L. Viviente. F. J. I. Oñate, M. Brizuela, A. Garcia-Luis, *ESMATS 2001 Proceedings* **2001**.
[26] I. Braceras, D. Gonzalez, J. I. Onate, M. Brizuela, J. L. Viviente, A. Garcı, I. Garmendia, **2007**, *85*, 75.
[27] M. Brizuela, J. I. Oñate, I. Garmendia, in *Proc. '13th European Space Mechanisms and Tribology Symposium – ESMATS 2009,'* **2009**, pp. 2–6.
[28] Y. Jing, J. Luo, S. Pang, **2004**, *461*, 288.
[29] R. Gilmore, M. A. Baker, P. N. Gibson, W. Gissler, M. Stoiber, P. Losbichler, C. Mitterer, **1998**, *109*, 345.
[30] Y. W. Bae, W. Y. Lee, T. M. Besmann, C. S. Yust, **1996**, *209*, 372.
[31] C. C. Baker, R. R. Chromik, K. J. Wahl, J. J. Hu, A. A. Voevodin, *Thin Solid Films* **2007**, *515*, 6737.
[32] C. C. Baker, J. J. Hu, A. A. Voevodin, *Surface and Coatings Technology* **2006**, *201*, 4224.
[33] A. A. Voevodin, T. A. Fitz, J. J. Hu, J. S. Zabinski, *Journal of Vacuum Science & Technology A: Vacuum, Surfaces, and Films* **2002**, *20*, 1434.
[34] C. C. Baker, **2014**, 1.
[35] M. C. Simmonds, A. Savan, E. Pflüger, H. van Swygenhoven, *Surface and Coatings Technology* **2000**, *126*, 15.
[36] P. Stoyanov, R. R. Chromik, D. Goldbaum, J. R. Lince, X. Zhang, *Tribology Letters* **2010**, *40*, 199.
[37] G. Colas, A. Saulot, E. Regis, Y. Berthier, *Wear* **2015**, *330–331*, 448.
[38] K. P. Furlan, J. D. B. de Mello, A. N. Klein, *Tribology International* **2018**, *120*, 280.
[39] H. Zhang, H. Tang, T. M. Yue, *International Journal of Metallurgical & Materials Engineering* **2018**, *4*, DOI 10.15344/2455-2372/2018/140.
[40] W. Hu, J. Xu, X. Lu, D. Hu, H. Tao, P. Munroe, Z. H. Xie, *Applied Surface Science* **2016**, *368*, 177.
[41] M. B. Peterson, R. L. Johnson, *FRICTION OF POSSIBLE SOLID LUBRICANTS WITH VARIOUS CRYSTAL STRUCTURES*, Washington, DC, **1954**.
[42] J. S. Przybyszewski, *A REVIEW OF LUBRICATION OF SLIDING-AND ROLLING-ELEMENT ELECTRICAL CONTACTS IN VACUUM*, Washington, DC, **1968**.
[43] D. J. Boes, *IEEE TRANSACTIONS ON AEROSPACE* **1964**, *2*, 457.
[44] K. Hebbar Kannur, T. Huminiuc, T. bin Yaqub, T. Polcar, C. Pupier, C. Héau, A. Cavaleiro, *Surface and Coatings Technology* **2021**, *408*, DOI 10.1016/j.surfcoat.2020.126791.

[45] P. Serles, H. Sun, G. Colas, J. Tam, E. Nicholson, G. Wang, J. Howe, A. Saulot, C. V. Singh, T. Filleter, *Advanced Materials Interfaces* **2020**, *1901870*, 1.
[46] J. A. Thornton, *Ann. Rev. Mater. Sci* **1977**, *7*, 239.
[47] G. Colas, A. Saulot, C. Godeau, Y. Michel, Y. Berthier, *Wear* **2013**, *305*, 192.
[48] B. C. Stupp, *Thin Solid Films* **1981**, *84*, 257.
[49] X. Qin, P. Ke, A. Wang, K. H. Kim, *Surface and Coatings Technology* **2013**, *228*, 275.
[50] W. R. Jones, S. v Pepper, A. Y. T. Corporation, B. Park, E. P. Kingsbury, S. H. Loewenthal, *Nasa Sti* **2000**, DOI 10.4271/2000-01-1828.
[51] A. J. John, S. C. Garcia, K. L. Kerrisk, M. J. Freeman, C. E. F. Clark, *Wear* **1993**, *162–164*, 614.
[52] G. Colas, Utilisation Raisonnée de Contaminants Pour Caractériser La Rhéologie Des 1ers et 3ème Corps Solides : Application à La Tribologie En Ambiances Spatiales, **2013**.
[53] H. Li, G. Zhang, L. Wang, *Journal of Physics D: Applied Physics* **2016**, *49*, DOI 10.1088/0022-3727/49/9/095501.
[54] Ö. Baran, F. Bidev, H. Çiçek, L. Kara, I. Efeoğlu, T. Küçükömeroğlu, *Surface and Coatings Technology* **2014**, *260*, 310.
[55] G. Colas, A. Saulot, D. Philippon, Y. Berthier, D. Léonard, *ACS Applied Materials and Interfaces* **2018**, *10*, 20106.
[56] D. Aldridge, M. Gentilhomme, A. Gibson, P. Cameron, A. Mccolgan, *Proceedings of the 16th European Space Mechanisms & Tribology Symposium - ESMATS 2015* **2015**, *2015*, 23.
[57] K. Miyoshi, *Solid Lubricants and Coatings for Extreme Environments : State-of-the-Art Survey*, Glenn Research Center, Cleaveland, Ohio, **2007**.
[58] L. B. Hall, *NASA Requirements for the Sterilization of Spacecraft*, National Aeronautics And Space Administration, Pasadena, California, **1965**.
[59] B. C. Windom, W. G. Sawyer, D. W. Hahn, *Tribology Letters* **2011**, *42*, 301.
[60] S. Domínguez-Meister, T. C. Rojas, M. Brizuela, J. C. Sánchez-López, *Science and Technology of Advanced Materials* **2017**, *18*, 122.
[61] B. D. Green, *Satellite Contamination and Materials Outgassing Knowledgebase*, Andover, Massachusetts, **2001**.
[62] M. Hässig, K. Altwegg, H. Balsiger, U. Calmonte, A. Jäckel, B. Schläppi, T. Sémon, P. Wurz, J. J. Berthelier, J. de Keyser, B. Fiethe, S. A. Fuselier, U. Mall, H. Rème, M. Rubin, in *2nd International Conference on Space Technology, ICST 2011*, **2011**.
[63] Y. Berthier, M. Godet, M. Brendle, *Tribology Transactions* **1989**, *32*, 490.
[64] G. Colas, S. Pajovic, A. Saulot, M. Renouf, P. Cameron, **2017**, pp. 20–22.
[65] V. Hegadekatte, S. Kurzenhäuser, N. Huber, O. Kraft, *Tribology International* **2008**, *41*, 1020.
[66] J. F. Archard, *Journal of Applied Physics* **1953**, *24*, 981.
[67] B. Chakraborty, H. S. S. R. Matte, A. K. Sood, C. N. R. Rao, *Journal of Raman Spectroscopy* **2013**, *44*, 92.
[68] N. T. McDevitt, J. E. Bultman, J. S. Zabinski, *Applied Spectroscopy* **1998**, *52*, 1160.
[69] F. Gustavsson, S. Jacobson, *Tribology International* **2016**, *101*, 340.
[70] J. Wang, K. C. Rose, C. M. Lieber, *Journal of Physical Chemistry B* **1999**, DOI 10.1021/jp9920794.
[71] T. Liang, W. G. Sawyer, S. S. Perry, S. B. Sinnott, S. R. Phillpot, *Physical Review B - Condensed Matter and Materials Physics* **2008**, *77*, DOI 10.1103/PhysRevB.77.104105.
[72] K. van Acker, K. Vercammen, *Wear* **2004**, *256*, 353.
[73] M. Sasaki, I. Nakamura, I. Takano, Y. Sawada, *Electrical Engineering in Japan (English translation of Denki Gakkai Ronbunshi)* **2004**, *149*, 1.

[74] W. Hu, J. Xu, X. Lu, D. Hu, H. Tao, P. Munroe, Z. H. Xie, *Applied Surface Science* **2016**, *368*, 177.
[75] Z. Ding, Q. Zhou, Y. Wang, Z. Ding, Y. Tang, Q. He, *Ceramics International* **2021**, *47*, 1133.
[76] O. D. Greenwood, S. C. Moulzolf, P. J. Blau, R. J. Lad, *Wear* **1999**, *232*, 84.
[77] N. M. U. Renevier, V. C. Fox, D. G. Teer, J. Hampshire, *Surface and Coatings Technology* **2000**, 24.
[78] S. Domínguez-Meister, T. C. Rojas, M. Brizuela, J. C. Sánchez-López, *Science and Technology of Advanced Materials* **2017**, *18*, 122.
[79] P. Yuan, C. Li, S. Xu, J. Liu, X. Wang, *Acta Materialia* **2017**, *122*, 152.
[80] W. C. Oliver, G. M. Pharr, *Journal of Materials Research* **1992**, *7*, 1564.
[81] G. Kresse, J. Furthmüller, *Physical review B* **1996**, *54*, 11169.
[82] G. Kresse, D. Joubert, *Physical Review B* **1999**, *59*, 1758.
[83] J. P. Perdew, K. Burke, M. Ernzerhof, *Physical review letters* **1996**, *77*, 3865.
[84] S. Grimme, J. Antony, S. Ehrlich, H. Krieg, *The Journal of chemical physics* **2010**, *132*, 154104.
[85] H. J. Monkhorst, J. D. Pack, *Physical review B* **1976**, *13*, 5188.
[86] A. Kerrigan, **2021**, DOI https://doi.org/10.5281/zenodo.5216942.
[87] A. Stukowski, *Modelling and Simulation in Materials Science and Engineering* **2010**, *18*, DOI 10.1088/0965-0393/18/1/015012.
[88] A. Jain, S. P. Ong, G. Hautier, W. Chen, W. D. Richards, S. Dacek, S. Cholia, D. Gunter, D. Skinner, G. Ceder, *APL materials* **2013**, *1*, 11002.